LETTER

doi:10.1038/nature12434

Asymmetric effects of daytime and night-time warming on Northern Hemisphere vegetation

Shushi Peng[1], Shilong Piao[1,2], Philippe Ciais[3], Ranga B. Myneni[4], Anping Chen[5], Frédéric Chevallier[3], Albertus J. Dolman[6], Ivan A. Janssens[7], Josep Peñuelas[8,9], Gengxin Zhang[2], Sara Vicca[7], Shiqiang Wan[10], Shiping Wang[2] & Hui Zeng[11]

Temperature data over the past five decades show faster warming of the global land surface during the night than during the day[1]. This asymmetric warming is expected to affect carbon assimilation and consumption in plants, because photosynthesis in most plants occurs during daytime and is more sensitive to the maximum daily temperature, T_{max}, whereas plant respiration occurs throughout the day[2] and is therefore influenced by both T_{max} and the minimum daily temperature, T_{min}. Most studies of the response of terrestrial ecosystems to climate warming, however, ignore this asymmetric forcing effect on vegetation growth and carbon dioxide (CO_2) fluxes[3–6]. Here we analyse the interannual covariations of the satellite-derived normalized difference vegetation index (NDVI, an indicator of vegetation greenness) with T_{max} and T_{min} over the Northern Hemisphere. After removing the correlation between T_{max} and T_{min}, we find that the partial correlation between T_{max} and NDVI is positive in most wet and cool ecosystems over boreal regions, but negative in dry temperate regions. In contrast, the partial correlation between T_{min} and NDVI is negative in boreal regions, and exhibits a more complex behaviour in dry temperate regions. We detect similar patterns in terrestrial net CO_2 exchange maps obtained from a global atmospheric inversion model. Additional analysis of the long-term atmospheric CO_2 concentration record of the station Point Barrow in Alaska suggests that the peak-to-peak amplitude of CO_2 increased by 23 ± 11% for a +1 °C anomaly in T_{max} from May to September over lands north of 51° N, but decreased by 28 ± 14% for a +1 °C anomaly in T_{min}. These lines of evidence suggest that asymmetric diurnal warming, a process that is currently not taken into account in many global carbon cycle models, leads to a divergent response of Northern Hemisphere vegetation growth and carbon sequestration to rising temperatures.

Both modelling and observational studies suggest that climate warming will probably enhance vegetation growth in northern terrestrial ecosystems, increasing carbon storage[3–6]. However, most of these studies do not consider the potential effects of asymmetric daytime and night-time warming. The increasing rate of global land-surface daily minimum temperature (T_{min}) over the past five decades is 1.4 times that of daily maximum temperature (T_{max})[1]. This asymmetric warming is expected to affect carbon assimilation and consumptions in plants, given that photosynthesis in most plants occurs during the daytime and thus is more sensitive to T_{max}, whereas plant respiration occurs throughout the whole day[2], and is therefore influenced by both T_{max} and T_{min}.

A few field experiments have been conducted to study the effects of asymmetric warming on ecosystems[7,8]. These and other direct field observations[9–11] reveal different effects of temperature during daytime and night time on vegetation growth and CO_2 fluxes. Yet the scarcity and short duration of field experiments makes it difficult to assess the large-scale response of vegetation to changes in T_{max} and T_{min}, which may differ between regions and ecosystems[7–10]. In this study, we use 28 years of satellite-derived NDVI data, global time-varying maps of land net CO_2 exchange (NCE) fluxes from an atmospheric inversion model, and *in situ* atmospheric CO_2 concentration measurements, together with T_{max} and T_{min} data (Methods) to study the spatial patterns of covariations between interannual changes in T_{min} and T_{max} and changes in the NDVI and NCE of northern ecosystems.

We first examine the linkage between T_{max} or T_{min} and growing-season NDVI (April to October). There is a high positive correlation between T_{max} and T_{min} (Supplementary Fig. 1), and we studied the apparent responses of NDVI to T_{max} and T_{min} with partial correlation analyses to remove the covariate effects between T_{max} and T_{min} (see Methods). When the effects of growing-season T_{min}, precipitation and solar radiation are removed in the partial correlation, the individual effect of growing-season T_{max} interannual changes on interannual NDVI shows remarkable spatial patterns (Fig. 1a, c). In most of the boreal zone (>50° N), cold mountain regions (such as the Tibetan plateau), and wet temperate regions (Japan and southern China), growing-season NDVI is positively correlated with growing-season T_{max}, with statistical significance at the 0.05 level for about 15% of the area north of 25° N (Supplementary Table 1). This relatively small percentage of area showing significant relationships can be explained by the nonlinear relationships between vegetation productivity and climate variables[12], the impact of non-growing-season factors such as frost frequency and snow depth[13,14], and the various factors controlling vegetation growth in different areas, which limit the prevalence of one dominant environmental factor such as T_{max} for vegetation growth to only a small proportion of the entire study area. For example, if we consider boreal regions where vegetation growth is limited by temperature[6,15,16], a significant positive partial correlation between growing-season NDVI and T_{max} is found in about 22% of the area (Supplementary Table 1). This positive partial covariation between growing-season T_{max} and NDVI is particularly pronounced in north-western North America and Siberia (Fig. 1a). In contrast, in drier temperate regions (such as western China, central Eurasia, central and southwestern North America), interannual T_{max} anomalies exhibit negative partial correlations with NDVI.

However, when the effects of growing-season T_{max}, precipitation, and solar radiation are removed, the partial correlation between growing-season T_{min} and NDVI is found to be negative over most boreal and wet temperate regions (Fig. 1b, d). In arid and semi-arid regions, particularly grasslands in central North America and temperate China, the growing-season NDVI is significantly positively correlated with T_{min} (Fig. 1b and Supplementary Table 2). These opposite responses of

[1]Sino-French Institute for Earth System Science, College of Urban and Environmental Sciences, Peking University, Beijing 100871, China. [2]Institute of Tibetan Plateau Research, Chinese Academy of Sciences, Beijing 100085, China. [3]Laboratoire des Sciences du Climat et de l'Environnement (LSCE), UMR CEA-CNRS, Batîment 709, CE, L'Orme des Merisiers, F-91191 Gif-sur-Yvette, France. [4]Department of Earth and Environment, Boston University, 675 Commonwealth Avenue, Boston, Massachusetts 02215, USA. [5]Department of Ecology and Evolutionary Biology, Princeton University, Princeton, New Jersey 08544-1003, USA. [6]Department of Earth Sciences, VU University Amsterdam, Boelelaan 1085, 1081 HV, Amsterdam, The Netherlands. [7]Department of Biology, University of Antwerp, Universiteitsplein 1, 2610 Wilrijk, Belgium. [8]Centre de Recerca Ecològica i Aplicacions Forestals (CREAF), Cerdanyola del Valles, Barcelona 08193, Catalonia, Spain. [9]Consejo Superior de Investigaciones Científicas (CSIC), Global Ecology Unit CREAF-CEAB-CSIC-UAB, Cerdanyola del Valles, Barcelona 08193, Catalonia, Spain. [10]College of Life Sciences, Henan University, Kaifeng 475001, China. [11]Peking University Shenzhen Graduate School, Shenzhen 518055, China.

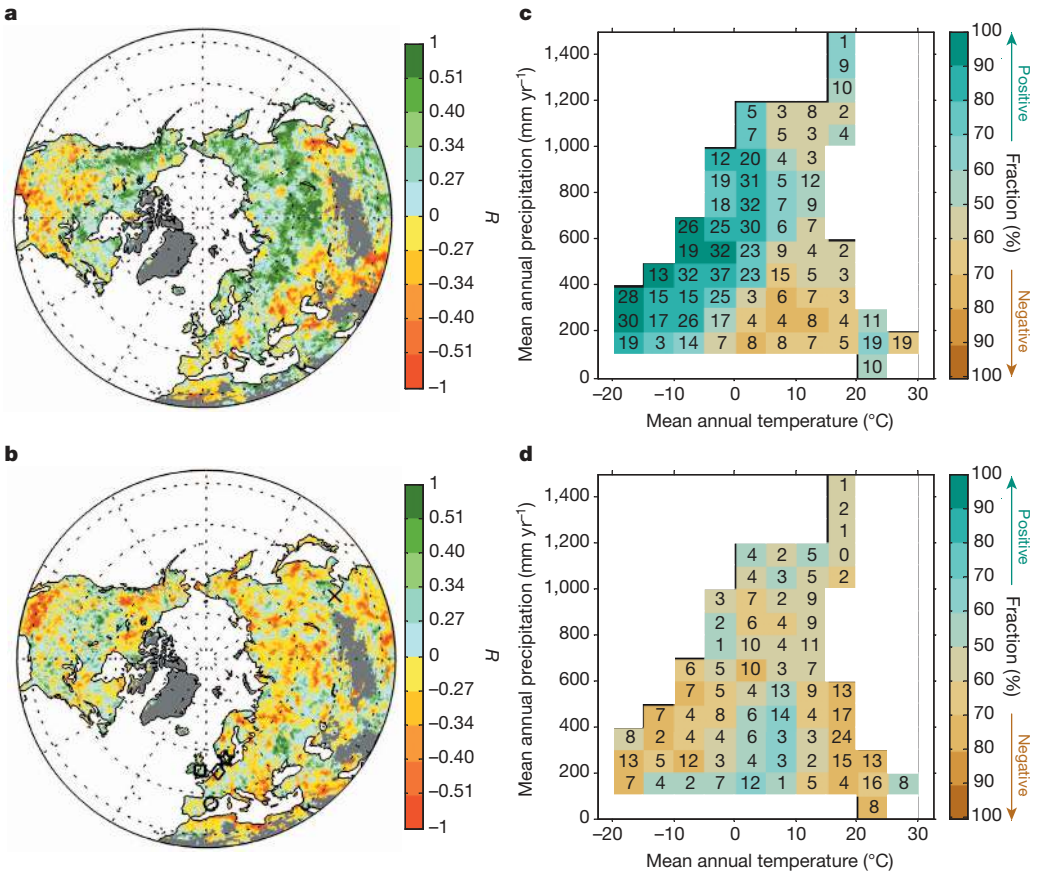

Figure 1 | The response of growing-season (from April to October) NDVI to changes in growing-season maximum temperature (T_{max}) and minimum temperature (T_{min}) in the Northern Hemisphere. **a**, Spatial distribution of the partial correlation coefficient R between growing-season NDVI and T_{max} after controlling for T_{min}, precipitation and solar radiation. **b**, Spatial distribution of R between growing-season NDVI and T_{min} after controlling for T_{max}, precipitation and solar radiation. The labels on the colour bars in **a** and **b**, $R = \pm 0.51$, $R = \pm 0.40$, $R = \pm 0.34$ and $R = \pm 0.27$ correspond to the 1%, 5%, 10% and 20% significance levels, respectively. Among the five night-time warming experiments sites marked in **b**, the results of four sites—Mols in Denmark (pentagram), Clocaenog in United Kindom (square), Garraf in Spain (circle) and Duolun in China (cross)—are consistent with the result of the partial correlation analysis between NDVI and T_{min} (Supplementary Table 2; the site of Oldebroek in the Netherlands was marked by a diamond in **b**). **c**, Percentage of pixels with dominant (positive pixels >50% or negative pixels >50%) partial correlation between NDVI and T_{max} (shown in **a**) in each 5 °C interval of mean annual temperature and 100-mm interval of mean annual precipitation climate space. **d**, Same as **c** but for the partial correlation between NDVI and T_{min} shown in **b**. The right colour bars in **c** and **d** indicate the fraction of pixels with dominant partial correlation between growing-season NDVI and T_{max}/T_{min}, and the numbers in each interval climate space of **c** and **d** indicate the percentage of pixels with significant partial correlation (for example, if the percentage of pixels with positive partial correlation exceeds 50%, the space is blue and the number is the percentage of pixels with positive and significant partial correlation, but if the percentage of pixels with positive partial correlation is less than 50%, the space is brown and the number is the percentage of pixels with negative and significant partial correlation).

NDVI to T_{min} between the wet and dry regions of the Northern Hemisphere is supported by some previous studies. For instance, an increase in T_{min} was found to reduce rice yields by 10% per °C in the Philippines[10], but to enhance growth at a temperate dry grassland site in China[8].

To test the robustness of our analysis, we also applied an independent statistical test called the ridge regression method[17]. The results show spatial patterns of the NDVI response to T_{max} and T_{min} similar to those obtained with a multiple-linear method (Supplementary Fig. 2). Nevertheless, the absolute magnitude of the sensitivities of NDVI to T_{max} and T_{min} is smaller in the ridge regression results. Patterns for the correlation between NDVI and T_{min} or T_{max} similar to those displayed in Fig. 1 were also obtained when using different growing-season definitions (May–October and May–September; Supplementary Figs 3 and 4), and using other gridded data sets of solar radiation, precipitation (or vapour pressure deficit as the moisture surrogate), instead of the climate data set from the Climate Research Unit (CRU) of the University of East Anglia, UK (Supplementary Figs 5–10). Finally, to test for possible spurious spatial correlations patterns that could be due to the spatial interpolation of meteorological station data in the CRU gridded data set, we performed the same correlation analyses using observed records from 1,736 individual meteorological stations available over the last three decades (Methods) and found the same pattern as in Fig. 1 (see Supplementary Figs 11 and 12).

Covariance between climate variables, regressed with NDVI, especially between T_{max} and T_{min} (Supplementary Fig. 1), could affect the interpretation of our partial correlation analyses. We therefore performed reduced partial correlation analyses separately using either T_{max}, precipitation and solar radiation or T_{min}, precipitation and solar radiation. The results show that the reduced partial correlation coefficients between NDVI and T_{min} (statistically controlling precipitation and solar radiation, but not T_{max}) have the same sign as between NDVI and T_{max} (statistically controlling precipitation and solar radiation, but not T_{min}), but with different strengths in most areas (Supplementary Fig. 13). In boreal ecosystems, the NDVI–T_{max} correlation is higher than the NDVI–T_{min} correlation, but in the dry temperate ecosystems it is lower. This result again confirms a differential response to warming; for example, boreal ecosystems respond more to increases in T_{max} than to increases in T_{min}.

Additionally, to minimize the effect of collinearity between T_{max} and T_{min} in a multiple linear regression statistical model, we also replaced them with their average ($T_{mean} = (T_{max} + T_{min})/2$) and difference

(DTR = $T_{max} - T_{min}$) and performed the same partial correlation analysis. The results show that boreal NDVI positively correlates with T_{mean} and DTR; whereas dry temperate NDVI exhibits negative relationships with T_{mean} and DTR (Supplementary Fig. 14). This is consistent with the results of partial correlation analysis with T_{max}, T_{min}, precipitation and solar radiation (Fig. 1). A statistical blind test also shows that the regression or partial correlation method used in our study correctly captures a relationship between NDVI and T_{max} or T_{min} if there is one (see Supplementary Information). Splitting the temperature signal into T_{max} and T_{min} thus helps the process interpretation of these results.

Second, we analysed how variations in T_{max} and T_{min} may influence interannual anomalies in the seasonal cycle of net CO_2 fluxes of northern ecosystems using the atmospheric CO_2 record of the stations of Point Barrow in Alaska (71° N) and Mauna Loa in Hawaii (19° N) (Methods). We found that the interannual variation in the amplitude of the detrended CO_2 seasonal cycle (AMP) at Point Barrow does not significantly correlate with the T_{mean} of May–September averaged over a broad boreal latitudinal zonal band (51°–90° N) ($R = -0.03$, $P = 0.897$); all variables were detrended and effects of precipitation and solar radiation were removed in the partial correlation analysis. This weak correlation of AMP with T_{mean}, however, masks its significant but opposite correlations with T_{max} and T_{min}. Indeed, multiple linear regression analyses, using AMP at Point Barrow as the dependent variable and detrended precipitation, solar radiation, T_{max} or T_{min} as independent variables, show that AMP responds positively to positive T_{max} anomalies by 3.8 ± 1.9 p.p.m. per °C (23 ± 11% of peak-to-peak AMP per °C of T_{max}) ($R = 0.38$, $P = 0.048$), but negatively to positive T_{min} anomalies by −4.8 ± 2.4 p.p.m. per °C (−28 ± 14% of peak-to-peak AMP per °C of T_{min} ($R = -0.38$, $P = 0.047$); Fig. 2 and Supplementary Table 3). At Mauna Loa, no significant partial correlation is obtained between interannual AMP variations and either the corresponding T_{max} ($R = -0.02$, $P = 0.866$) or the corresponding T_{min} ($R = 0.02$, $P = 0.893$) variations (Fig. 2), possibly owing to the mixed temperature effects across different temperate regions (Fig. 1).

Last, we investigated the covariance between the interannual anomalies of NCE (positive values indicating net CO_2 uptake by ecosystems) and those of T_{max} and T_{min} using NCE gridded estimates from a global atmospheric inversion over the last three decades[18]. For the boreal region (>50° N), the inversion-based NCE from May to September is found to respond positively to positive anomalies of T_{max}, with a sensitivity of 1.1 ± 0.6 Pg of C per °C ($R = 0.37$, $P = 0.059$), and negatively to positive anomalies of T_{min}, with a sensitivity of −1.7 ± 0.7 Pg of C per °C ($R = -0.45$, $P = 0.021$; Fig. 3 and Supplementary Table 4) (1 Pg = 10^{15} g). These relationships are qualitatively similar to the ones found between AMP versus T_{max} and T_{min} in the boreal zone. In the temperate latitude band (25°–50° N), the inversion-based NCE from May to October is not significantly correlated with either T_{max} ($R = 0.11$, $P = 0.604$) or T_{min} ($R = -0.24$, $P = 0.238$) (Fig. 3). Similar patterns were also obtained when using the inversion with flat prior information (Supplementary Fig. 15). Note that inversion NCE uncertainties are large at the grid-point scale, and that individual grid point NCE estimates are correlated with each other. The spatial distribution of the response of inversion NCE to T_{max} and T_{min} over the climatic dimensions (Supplementary Figs 16 and 17) is comparable with that derived from the (independent) NDVI (Fig. 1c and d). Interestingly, the geographical area where the growing-season NCE positively correlates with T_{max} (Supplementary Figs 16 and 17) is less extensive than the area where growing-season NDVI positively correlates with T_{max} (Fig. 1). This could be explained by a concurrent increase of soil organic matter decomposition induced by warming in boreal and temperate regions where water is readily available.

In summary, our analyses of several data streams consistently point out that interannual changes in growing-season T_{max} and T_{min} have regionally opposite effects on NDVI (greenness) and NCE. Daytime positive T_{max} anomalies correlate positively with enhanced photosynthetic activity (NDVI) and NCE over wet and cool ecosystems, but have negative effects in dry temperate regions. These regionally contrasting effects of T_{max} interannual variations on interannual vegetation greenness and growing-season CO_2 uptake are most probably associated with different ecophysiological responses. In boreal regions, photosynthetic activity and NCE are subject to temperature limitation but less subject to water limitation[6,15,16]. Rising T_{max} has been observed to enhance photosynthetic enzyme activity[19], to increase soil nitrogen mineralization and availability[20], and to extend the growing season[21]. In contrast, in dry temperate regions where soil water limitation can limit vegetation growth, daytime warming can reduce photosynthetic activity through enhanced evaporation, and reduced soil water content[8]. The hypothesis that a drop in topsoil water content (SWC) below a critical stress level in dry temperate regions is associated with warmer T_{max} during the growing season is consistent with the negative partial correlation coefficients between growing-season T_{max} and SWC retrieved from multiple microwave satellite sounders over 1988–2007 (ref. 22) (Fig. 4a, Supplementary Figs 18–21).

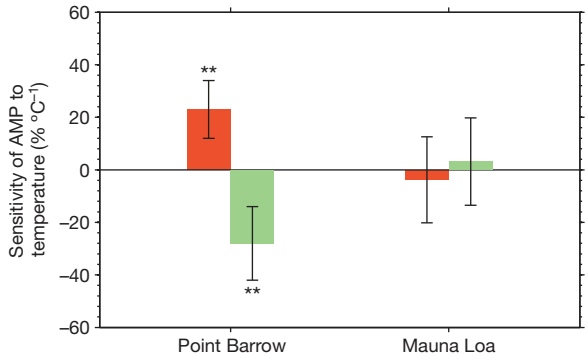

Figure 2 | T_{max} and T_{min} sensitivity of annual AMP at Point Barrow and Mauna Loa stations. The T_{max} (red) and T_{min} (green) sensitivity of AMP at each station was estimated based on a multiple linear regression analysis using detrended AMP as the dependent variable and the detrended precipitation, solar radiation, T_{max} and T_{min} during the corresponding season (May–September for Point Barrow station and May–October for Mauna Loa station) over a broad region surrounding each station by ±20 degrees of latitude (51°–90° N for Point Barrow and 1° S–39° N for Mauna Loa) as the independent variables. **Statistically significant at the 95% ($P < 0.05$) level. The error bars are standard errors of the mean of the corresponding parameters.

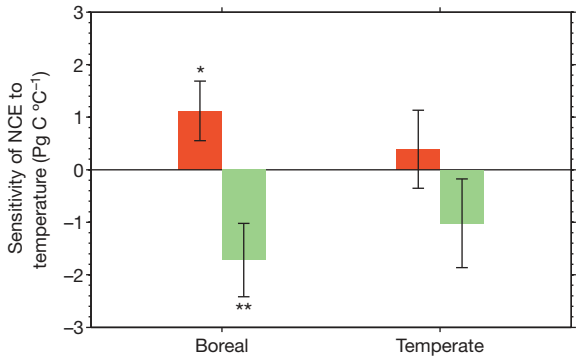

Figure 3 | T_{max} and T_{min} sensitivity of a global atmospheric inversion model estimated NCE in boreal and temperate regions. Using an approach similar to that of Fig. 2, we calculated the sensitivity of corresponding season NCE in boreal (50°–90° N) and temperate (25°–50° N) regions to changes in T_{max} and T_{min} (May–September for boreal regions and May–October for temperate regions). The T_{max} (red) and T_{min} (green) sensitivity of NCE was calculated based on a multiple linear regression analysis using detrended NCE as the dependent variable and the detrended corresponding precipitation, solar radiation, T_{max} and T_{min} as the independent variables. *Statistically significant at the 90% ($P < 0.1$) level; **Statistically significant at the 95% ($P < 0.05$) level. The error bars are standard errors of the mean of the corresponding parameters.

Night-time warming can influence vegetation productivity in two opposite ways: via enhanced autotrophic respiration, and indirectly via stimulation of plant photosynthesis during the following daytime through decreasing frost risk[13,23], and physiological regulatory mechanisms[8,11,19,24]. Leaf carbohydrates synthesized during the daytime were observed to be consumed more quickly during warmer nights because of enhanced leaf respiration[19,24], which depletes foliar carbohydrates and may produce a rebound effect of compensatory stimulated photosynthesis during the following day[8,19]. This mechanism could partly explain the positive partial correlation between NDVI and T_{min} in temperate grassland regions[8]. In contrast, the observed decrease in vegetation activity associated with warmer T_{min} in boreal and in wet temperate regions implies that the negative impact of increased autotrophic respiration is more dominant in these regions, but further studies are needed to support these inferences. In addition, changes in T_{min} could influence vegetation productivity through shifting competitive interactions among C_3 and C_4 plants in semi-arid biomes with warm summer conditions[9].

The asymmetrical response of terrestrial ecosystems to daytime versus night-time temperature anomalies found in this study suggests that most of the currently used global carbon cycle models using daily temperature forcing may neglect an essential process. If the night-time warming trend observed over the last five decades continues to be faster than that of daytime warming[1], the model using average daily temperature may overestimate the increase of boreal vegetation productivity by the end of this century[25]. Arguably, many terrestrial ecosystem models[26,27] using daily or monthly temperature data as input will not capture the response of vegetation to asymmetric diurnal temperature changes, indicating the importance of understanding the diurnal cycle of CO_2 and energy fluxes in land biosphere models. This understanding could be achieved by pattern analysis of existing eddy-covariance flux measurements[28], targeted ecosystem manipulative experiments under controlled and different T_{min} and T_{max} conditions, as well as by mesocosm studies.

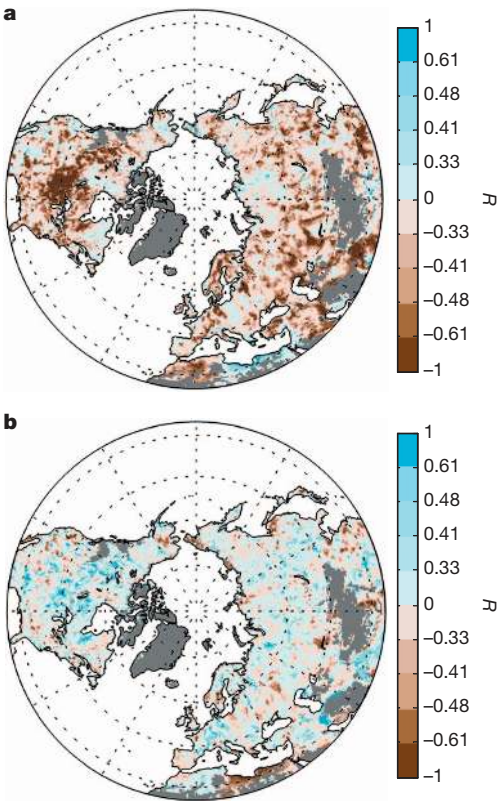

Figure 4 | The response of growing-season (April–October) SWC to changes in growing-season T_{max} and T_{min} in the Northern Hemisphere. **a**, Spatial distribution of the partial correlation coefficient R between growing-season SWC and T_{max}. **b**, Spatial distribution of the partial correlation coefficient R between growing-season SWC and T_{min}. R between growing-season SWC and T_{max} or T_{min} was calculated using the same approach for estimating R between growing-season NDVI and T_{max} or T_{min} in Fig. 1. The labels on the colour bars in **a** and **b**, $R = \pm 0.61$, $R = \pm 0.48$, $R = \pm 0.41$ and $R = \pm 0.33$ correspond to the 1%, 5%, 10% and 20% significance levels, respectively. Compared to the daytime warming effects, night-time warming exhibits a smaller negative correlation with SWC. The areas with positive correlation between SWC and T_{min} is 59% (significant over 6% of the areas). The observed positive correlation between T_{min} and SWC, particularly over the boreal and wet temperate regions, could be attributed in part to a decrease in evapotranspiration driven by a decrease in vegetation photosynthetic activity (or leaf area index), because higher T_{min} is generally accompanied by lower growing-season NDVI over these regions (Fig. 1).

METHODS SUMMARY

Satellite derived NDVI data were used to investigate the effects of daytime and night-time warming on the vegetation activity of Northern Hemispheric ecosystems. Then NCE values simulated from an inversion model, as well as from atmospheric CO_2 concentrations at Point Barrow and Mauna Loa stations, were used to investigate the response of the carbon balance to changes in T_{max} and T_{min}. Finally, the response of satellite-derived surface SWC to T_{max} and T_{min} were analysed to understand the mechanisms of asymmetric effects of daytime and night-time warming on Northern Hemisphere vegetation activity and carbon cycle. We applied a partial correlation analysis to statistically remove the effects of other factors, such as precipitation and solar radiation (all variables detrended); and the results were verified with those from another independent statistical method, ridge regression.

Full Methods and any associated references are available in the online version of the paper.

Received 15 October 2012; accepted 4 July 2013.

1. Solomon, S., *et al.* (eds) *Climate Change 2007: The Physical Science Basis. Contribution of Working Group I to the Fourth Assessment Report of the Intergovernmental Panel on Climate Change* (Cambridge Univ. Press, 2007).
2. Atkin, O. *et al.* Light inhibition of leaf respiration as soil fertility declines along a post-glacial chronosequence in New Zealand: an analysis using the Kok method. *Plant Soil* **367,** 163–182 (2013).
3. Keeling, R. F., Piper, S. C. & Heimann, M. Global and hemispheric CO_2 sinks deduced from changes in atmospheric O_2 concentration. *Nature* **381,** 218–221 (1996).
4. Myneni, R. B., Keeling, C. D., Tucker, C. J., Asrar, G. & Nemani, R. R. Increased plant growth in the northern high latitudes from 1981 to 1991. *Nature* **386,** 698–702 (1997).
5. Zhou, L. M. *et al.* Variations in northern vegetation activity inferred from satellite data of vegetation index during 1981 to 1999. *J. Geophys. Res.* **106,** 20069–20083 (2001).
6. Nemani, R. R. *et al.* Climate-driven increases in global terrestrial net primary production from 1982 to 1999. *Science* **300,** 1560–1563 (2003).
7. Beier, C. *et al.* Carbon and nitrogen cycles in European ecosystems respond differently to global warming. *Sci. Total Environ.* **407,** 692–697 (2008).
8. Wan, S., Xia, J., Liu, W. & Niu, S. Photosynthetic overcompensation under nocturnal warming enhances grassland carbon sequestration. *Ecology* **90,** 2700–2710 (2009).
9. Alward, R. D., Detling, J. K. & Milchunas, D. G. Grassland vegetation changes and nocturnal global warming. *Science* **283,** 229–231 (1999).
10. Peng, S. *et al.* Rice yields decline with higher night temperature from global warming. *Proc. Natl Acad. Sci. USA* **101,** 9971–9975 (2004).
11. Prasad, P. V. V., Pisipati, S. R., Ristic, Z., Bukovnik, U. & Fritz, A. K. Impact of night-time temperature on physiology and growth of spring wheat. *Crop Sci.* **48,** 2372–2380 (2008).
12. Zhou, L., Kaufmann, R. K., Tian, Y., Myneni, R. B. & Tucker, C. J. Relation between interannual variations in satellite measures of northern forest greenness and climate between 1982 and 1999. *J. Geophys. Res.* **108,** 4004, doi:10.1029/2002JD002510 (2003).
13. Kim, Y., Kimball, J. S., Zhang, K. & McDonald, K. C. Satellite detection of increasing Northern Hemisphere non-frozen seasons from 1979 to 2008: implications for regional vegetation growth. *Remote Sens. Environ.* **121,** 472–487 (2012).
14. Kreyling, J. Winter climate change: a critical factor for temperate vegetation performance. *Ecology* **91,** 1939–1948 (2010).
15. Beer, C. *et al.* Terrestrial gross carbon dioxide uptake: global distribution and covariation with climate. *Science* **329,** 834–838 (2010).
16. Lucht, W. *et al.* Climatic control of the high-latitude vegetation greening trend and Pinatubo effect. *Science* **296,** 1687–1689 (2002).
17. Hoerl, A. E. & Kennard, R. W. Ridge regression — biased estimation for nonorthogonal problems. *Technometrics* **12,** 55–67 (1970).

18. Chevallier, F. *et al.* CO_2 surface fluxes at grid point scale estimated from a global 21 year reanalysis of atmospheric measurements. *J. Geophys. Res.* **115,** D21307 (2010).
19. Turnbull, M. H., Murthy, R. & Griffin, K. L. The relative impacts of day-time and night-time warming on photosynthetic capacity in *Populus deltoides*. *Plant Cell Environ.* **25,** 1729–1737 (2002).
20. Melillo, J. M. *et al.* Soil warming and carbon-cycle feedbacks to the climate system. *Science* **298,** 2173–2176 (2002).
21. Menzel, A. *et al.* European phenological response to climate change matches the warming pattern. *Glob. Change Biol.* **12,** 1969–1976 (2006).
22. Owe, M., de Jeu, R. & Holmes, T. Multisensor historical climatology of satellite-derived global land surface moisture. *J. Geophys. Res.* **113,** F01002, doi: 10.1029/2007JF000769 (2008).
23. Gu, L. *et al.* The 2007 eastern US spring freezes: increased cold damage in a warming world? *Bioscience* **58,** 253–262 (2008).
24. Griffin, K. L. *et al.* Leaf respiration is differentially affected by leaf vs. stand-level night-time warming. *Glob. Change Biol.* **8,** 479–485 (2002).
25. Qian, H., Joseph, R. & Zeng, N. Enhanced terrestrial carbon uptake in the Northern High Latitudes in the 21st century from the Coupled Carbon Cycle Climate Model Intercomparison Project model projections. *Glob. Change Biol.* **16,** 641–656 (2010).
26. Potter, C. S. *et al.* Terrestrial ecosystem production—a process model based on global satellite and surface data. *Glob. Biogeochem. Cycles* **7,** 811–841 (1993).
27. Sitch, S. *et al.* Evaluation of ecosystem dynamics, plant geography and terrestrial carbon cycling in the LPJ dynamic global vegetation model. *Glob. Change Biol.* **9,** 161–185 (2003).
28. Baldocchi, D. 'Breathing' of the terrestrial biosphere: lessons learned from a global network of carbon dioxide flux measurement systems. *Aust. J. Bot.* **56,** 1–26 (2008).

Supplementary Information is available in the online version of the paper.

Acknowledgements This study was supported by the National Natural Science Foundation of China (grant numbers 41125004 and 31021001), the National Basic Research Program of China (grant numbers 2010CB950601 and 2013CB956303), the Foundation for Sino-EU Research Cooperation of the Ministry of Science and Technology of China (grant number 1003), and a Chinese Ministry of Environmental Protection Grant (number 201209031). We also acknowledge the GLOBALVIEW-CO_2 project based at NOAA ESRL. S.V. is a postdoctoral research associate of the Fund for Scientific Research (Flanders).

Author Contributions S. Piao, S. Peng and H.Z. designed the research. S. Peng performed analysis and calculations. S. Piao, P.C., A.C. and S. Peng drafted the paper. R.B.M. provided the remotely sensed NDVI data and contributed to the text. F.C. provided the atmospheric inverse model estimated carbon flux and contributed to the text. A.J.D. provided the remotely sensed soil moisture data and contributed to the text. I.A.J., J.P., G.Z., S.V., S. Wan, S. Wang and H.Z. contributed to the interpretation of the results and to the text.

Author Information Reprints and permissions information is available at www.nature.com/reprints. The authors declare no competing financial interests. Readers are welcome to comment on the online version of the paper. Correspondence and requests for materials should be addressed to S. Piao (slpiao@pku.edu.cn) or H.Z (zengh@pkusz.edu.cn).

METHODS

Satellite NDVI measurements. NDVI is defined as the ratio of the difference between near-infrared reflectance and red visible reflectance to their sum, and is a remote-sensed vegetation index widely used as an indicator of vegetation gross primary productivity[4,5]. The NDVI third-generation (NDVI3g) data used in this study were from the Global Inventory Monitoring and Modelling Studies (GIMMS) group derived from the NOAA/AVHRR land data set, at a spatial resolution of $8 \times 8\,km^2$ and 15-day interval, for the period January 1982 to December 2009 (ref. 29). The GIMMS-NDVI data set has been widely used for detecting vegetation growth change[5,29].

Atmospheric CO_2 measurements at two long-term monitoring stations. Weekly and monthly averaged atmospheric CO_2 concentrations at Point Barrow and Mauna Loa stations, based on continuous *in situ* observations, were obtained from the Earth System Research Laboratory of the National Oceanic and Atmospheric Administration (NOAA) (http://www.esrl.noaa.gov/gmd/ccgg/globalview). Atmospheric CO_2 concentration *in situ* station samples at Point Barrow and Mauna Loa cover the period 1979–2009 and 1959–2009, respectively.

NCE distribution from an atmospheric inversion. We use a global Bayesian inversion of NCE (a positive value indicates carbon uptake) over the past three decades[18]. Weekly CO_2 fluxes are estimated on each grid-point of a $3.75^\circ \times 2.5^\circ$ (longitude–latitude) global grid throughout the 29 years[18]. The inversion of NCE accounts for a priori time and space error correlations of NCE fluxes defined over land from the misfit between eddy-covariance observations and model simulations[18], and based on more than 128 individual atmospheric CO_2 measurements from flask and continuous-atmospheric-measurement sites (list in ref. 18). This inversion has been chosen because (1) NCE fluxes are estimated at relatively high spatial resolution for a global inversion, thus reducing the risk of spatial aggregation errors, (2) it is informed by high-temporal-resolution CO_2 measurements instead of monthly smoothed data, and (3) it covers a longer period than the TRANSCOM inversions[30], with 1981 as the beginning of the assimilation period. In addition, an inversion of NCE with a climatology of model simulations of NCE (without any interannual variations) as prior information over land was also used (Supplementary Fig. 15).

Climate data. The monthly T_{min}, T_{max} and precipitation data sets with spatial resolution of 0.5° used in this study are the CRU TS 3.1 climate data sets[31], covering NDVI, atmospheric CO_2 concentration and inversed CO_2 surface flux time series period (1959–2009). The CRU TS3.1 climate data sets are interpolated from meteorological stations based on spatial autocorrelation functions[31,32]. Because of the high spatial correlation in the interpolated CRU data sets[32], we also tested the robustness of our results with observed climate records from 1,736 individual meteorological stations (ftp://ftp.ncdc.noaa.gov/pub/data/gsod/).

Solar radiation was obtained from the CRU–NCEP data set (the period 1901–2009), which is based on the combination of the CRU TS 3.1 climate data set covering the period 1901–2009 and the NCEP reanalysis covering the period 1948–2009 (http://nacp.ornl.gov/thredds/fileServer/reccapDriver/cru_ncep/analysis/readme.htm). To assess whether the relationships between vegetation production and T_{max} and T_{min} are robust across different data sets, we also used two satellite-based solar radiation data sets—ISCCP[33] and the NASA/GEWEX Surface Radiation Budget, http://gewex-srb.larc.nasa.gov/common/php/SRB_data_products.php—covering the period 1984–2007, three precipitation data sets—GPCP[34], GPCC (http://gpcc.dwd.de) and precipitation from ref. 35—and the vapour pressure deficit calculated from CRU TS 3.1 (ref. 36).

Soil water content data. Daily SWC data ($m^3\,m^{-3}$) with spatial resolution of 0.25° over the period 1988–2007 was derived from the Special Sensor Microwave/Imager satellite using the Land Parameter Retrieval Model, which solves simultaneously for the SWC and vegetation optical depth[22]. This data set has been validated extensively over a large variety of land surfaces of sparse to moderate vegetation, showing good agreement with *in situ* observations[37].

Analyses. Several of the environmental variables tested as predictors of NDVI or NCE covary with one another. This covariance needs to be carefully dealt with when we want to detect the relationship between the dependent variable and one particular independent variable. In evaluating the relationship between NDVI or NCE and T_{max} or T_{min}, we used partial correlation analyses to exclude the confounding effects of other variables. Partial correlation analysis is a widely applied statistical tool to isolate the relationship between two variables from the confounding effects of many correlated variables[15,38,39].

To verify the asymmetric diurnal warming effect on vegetation growth derived from partial correlation analysis, we also performed a ridge regression analysis[17]. Ridge regression is a linear regularization method and constrained linear inversion method, which reduces the size of the regression coefficients by introducing a constant in the minimized residual equation[17]. The analysis was performed in the R package lm.ridge with an HKB estimate of the ridge constant (ref. 40, http://astrostatistics.psu.edu/su07/R/html/MASS/html/lm.ridge.html). We also performed the partial correlation analysis by replacing T_{max} and T_{min} with their average ($T_{mean} = (T_{max} + T_{min})/2$) and difference ($DTR = T_{max} - T_{min}$). Additionally, we conducted reduced partial correlation analyses in which the dependent variables were correlated twice: once against T_{max}, precipitation and solar radiation, and once against T_{min}, precipitation and solar radiation.

We used averages of monthly NDVI data during the growing season to study the response of vegetation growth to temperature. To match NDVI data (8 km spatial resolution) with climate data (0.5° spatial resolution), we averaged monthly NDVI data corresponding to each climate data set pixel. Monthly NDVI was obtained by choosing the monthly maximum value, which can further eliminate the disturbance from cloud, atmosphere and changes in solar altitude angle[4,5]. Following a previous study[5], growing season is defined as the period from April to October. We also used different growing-season definitions (from May to October and from May to September) in the Supplementary Information. The sensitivity of growing-season NDVI to changes in T_{max} and T_{min} was estimated based on multiple linear regression analysis using growing-season NDVI as the dependent variable and the corresponding precipitation, solar radiation, T_{max}, and T_{min} as independent variables (all variables detrended). Similarly, we also calculated the sensitivity of growing-season NCE and SWC to changes in T_{max} and T_{min}. After aggregation of daily SWC data into monthly means, the sensitivity of growing-season SWC to changes in T_{max} and T_{min} was calculated only in those pixels where SWC was recorded at least three months during the growing season. The average number of days with available daily SWC data per month during the growing season for each pixel was shown in Supplementary Fig. 22.

We used the curve-fitting procedures (CCGVU program)[41] to extract the detrended seasonal cycle from the monthly atmospheric CO_2 concentration record at Point Barrow and Mauna Loa stations. The annual maximum concentrations in the mean seasonal cycle were recorded at May for both Point Barrow and Mauna Loa, whereas the annual minimum concentrations in the mean seasonal cycle were recorded at August/September and September/October for Point Barrow and Mauna Loa, respectively. AMP is calculated as the difference between the annual maximum and minimum concentrations for each station. The temperature sensitivity of AMP at each station was estimated based on multiple linear regression analysis using detrended AMP as the dependent variable and the detrended precipitation, solar radiation, T_{max} and T_{min} during the corresponding season (from May to September for Point Barrow station and from May to October for Mauna Loa station) over a broad region surrounding each station by ± 20 degrees of latitude as independent variables. The regional climate variables were weighted by mean annual MODIS net primary production over 2000–2009 (ref. 42) to focus on the vegetated areas. Using a similar approach, we also calculated the sensitivity of corresponding season NCE in boreal (50°–90° N) and temperate (25°–50° N) regions to changes in T_{max} and T_{min} (May–September for boreal regions and May–October for temperate regions). The uncertainties of the sensitivity were estimated based on the standard errors of the corresponding parameters.

29. Tucker, C. J. *et al.* An extended AVHRR 8-km NDVI dataset compatible with MODIS and SPOT vegetation NDVI data. *Int. J. Remote Sens.* **26,** 4485–4498 (2005).
30. Baker, D. F. *et al.* TransCom 3 inversion intercomparison: impact of transport model errors on the interannual variability of regional CO_2 fluxes, 1988-2003. *Glob. Biogeochem. Cycles* **20,** GB1002 (2006).
31. Mitchell, T. D. & Jones, P. D. An improved method of constructing a database of monthly climate observations and associated high-resolution grids. *Int. J. Climatol.* **25,** 693–712 (2005).
32. New, M., Hulme, M. & Jones, P. Representing twentieth-century space–time climate variability. Part II: Development of 1901–96 monthly grids of terrestrial surface climate. *J. Clim.* **13,** 2217–2238 (2000).
33. Zhang, Y., Rossow, W. B. & Stackhouse, P. W. Comparison of different global information sources used in surface radiative flux calculation: radiative properties of the near-surface atmosphere. *J. Geophys. Res.* **111,** D13106 (2006).
34. Adler, R. F. *et al.* The version-2 global precipitation climatology project (GPCP) monthly precipitation analysis (1979–present). *J. Hydrometeorol.* **4,** 1147–1167 (2003).
35. Willmott, K. & Matsuura, C. J. *Terrestrial Precipitation: 1900–2008 Gridded Monthly Time Series* http://climate.geog.udel.edu/~climate/html_pages/Global2_Ts_2009/README.global_p_ts_2009.html (accessed 20 January 2013).
36. Prenger, J. J. & Ling, P. P. *Greenhouse Condensation Control: Understanding and Using Vapor Pressure Deficit (VPD)* http://ohioline.osu.edu/aex-fact/0804.html (accessed 20 January 2013).
37. de Jeu, R. A. M. *et al.* Global soil moisture patterns observed by space borne microwave radiometers and scatterometers. *Surv. Geophys.* **29,** 399–420 (2008).
38. Behera, S. K. *et al.* Paramount impact of the Indian Ocean dipole on the East African short rains: A CGCM study. *J. Clim.* **18,** 4514–4530 (2005).
39. Wang, H., Wang, B., Huang, F., Ding, Q. G. & Lee, J. Y. Interdecadal change of the boreal summer circumglobal teleconnection (1958-2010). *Geophys. Res. Lett.* **39,** L12704, doi:10.1029/2012gl052371 (2012).
40. Hoerl, A. E., Kennard, R. W. & Baldwin, K. F. Ridge regression—some simulations. *Commun. Stat. Theor. Med.* **4,** 105–123 (1975).

41. Thoning, K. W., Tans, P. P. & Komhyr, W. D. Atmospheric carbon dioxide at Mauna Loa observatory 2. analysis of the NOAA GMCC data, 1974-1985. *J. Geophys. Res.* **94,** 8549–8565 (1989).

42. Zhao, M. S. & Running, S. W. Drought-induced reduction in global terrestrial net primary production from 2000 through 2009. *Science* **329,** 940–943 (2010).